Pergamon

Journal of Structural Geology, Vol. 19, Nos 3–4, pp. 337 to 354, 1997

PII: S0191-8141(96)00118-6
0191-8141/97 $17.00 + 0.00

Detachment folds with fixed hinges and variable detachment depth, northeastern Brooks Range, Alaska

THOMAS X. HOMZA* and WESLEY K. WALLACE

Tectonics and Sedimentation Research Group, Department of Geology and Geophysics and Geophysical Institute, University of Alaska, Fairbanks, AK 99775-5780, U.S.A.

(*Received* 2 *February* 1996; *accepted in revised form* 8 *October* 1996)

Abstract—Detachment anticlines in the northeastern Brooks Range accommodated displacement above a detachment by buckling of a competent unit over an incompetent unit. Meso- and microstructures in hinges and a lack of relict hinge structures in limbs suggest that these folds grew with fixed hinges. The structural thickness of the incompetent unit beneath the folds (detachment depth) varies from less than to greater than the stratigraphic thickness. A model in which incompetent unit thickness varies with fold area better approximates the geometry of the folds than does a more conventional constant-depth model. Additional discrepancies between modelled and observed incompetent unit thickness and field observations suggest non-plane strain and/or transport of material through the boundaries of the fold in the plane of the cross-section.

The results of this study suggest a typical evolutionary sequence for detachment folds in the northeastern Brooks Range, which may be applicable elsewhere. Anticlines initiate as fixed-hinge buckle folds. Rapid initial increase in anticlinal cross-sectional area results in a decrease in incompetent unit thickness. Fold area begins to decrease with tightening beyond an interlimb angle of 90°. Decreasing fold area is accommodated through some combination of structural thickening of the incompetent unit, transport of solid or dissolved material out of the plane of section, transport of material through the boundaries of the fold in the plane of the cross-section, and/or truncation by thrust faults.

INTRODUCTION

A detachment fold (Jamison, 1987; Mitra and Namson, 1989; Dahlstrom, 1990; Groshong and Epard, 1994; Homza and Wallace, 1995; Epard and Groshong, 1995; Poblet and McClay, 1996) is defined by a relatively competent rock layer that is separated by an internally deformed, less-competent interval from a detachment surface or zone across which most of the fold shortening has been accommodated (Fig. 1). Mechanically layered stratigraphy characterized by distinct competent and incompetent units is very common in fold-and-thrust belts and lends itself to the formation of detachment folds. Thus, it is likely that detachment folds are at least as common in fold-and-thrust belts as 'rigid-ramp' folds such as fault-bend (Suppe, 1983; Jamison, 1987) or fault-propagation folds (Jamison, 1987; Mitra, 1990; Suppe and Medwedeff, 1990). However, due to the relatively unconstrained behavior of incompetent rock, the geometry and kinematics of detachment folds are more complex and less well understood than for fault-bend or fault-propagation folds (Homza and Wallace, 1995; Poblet and McClay, 1996). Models for fault-bend and fault-propagation folds are more widely known and used than those for detachment folds, and a clear and consistent definition of detachment folds is not in general use. Many detachment folds probably have been described in the scientific literature, but are not explicitly identified as such. Thus, we believe detachment folds are more common than the scientific literature would suggest, but commonly are misinterpreted as fault-bend or fault-propagation folds.

This paper addresses three fundamental yet unresolved questions about detachment folds that must be addressed in order to enable both their recognition and reliable geometric and kinematic interpretation, especially in the subsurface. First, do detachment folds form with fixed hinges and rotating limbs (e.g. Hardy and Poblet, 1994), with migrating hinges and non-rotating limbs (e.g. Mitra and Namson, 1989), or with some combination of fixed and migrating hinges (e.g. Poblet and Hardy, 1995)? Second, does the thickness of the incompetent unit (or depth-to-detachment) vary structurally during folding and, if so, is it possible to predict the amount of such variation? Third, what role in detachment folding is played by differences in competency resulting from variations in rock type, bed thickness, and interbedding within a multi-layered mechanical stratigraphy? To address these questions, we have made map-, outcrop-, and microscopic-scale observations of well-exposed natural detachment folds and analyzed these folds using the 'variable detachment-depth model' (VDDM) (Homza and Wallace, 1995). Most previously published models for detachment folds require that detachment depth remain constant, that hinges migrate, or both (e.g. Jamison, 1987; Mitra and Namson, 1989; Dahlstrom, 1990; Epard and Groshong, 1995), and these assumptions exclude a range of other possible kinematic models (e.g. Homza and Wallace, 1995; Poblet and McClay, 1996). The VDDM does not require that detachment depth remain constant or that hinges migrate and this flexibility has allowed us to use the VDDM primarily as a

*Present address: BP Exploration (Alaska) Inc., P.O. Box 196612, 900 E. Benson Blvd, Anchorage, AK 99519, U.S.A.

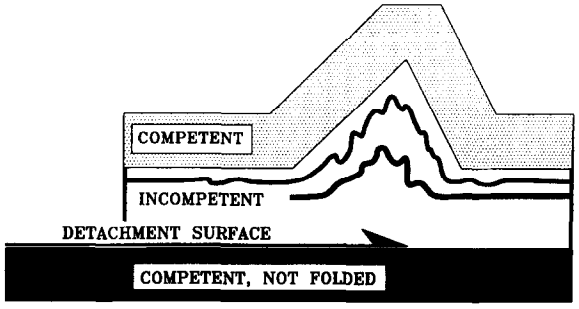

Fig. 1. An idealized model of a detachment fold showing the essential mechanical stratigraphy, which consists of two competent units separated by an incompetent unit.

tool to analyze the geometry and kinematics of particular detachment folds.

All of the folds we observed are best described kinematically as fixed-hinge (fixed arc-length) buckle folds because the geometry and distribution of strain-indicators in each fold are incompatible with a migrating-hinge mechanism. Structural changes in both incompetent unit thickness (depth-to-detachment) and cross-sectional area are required by the observed fold geometries and are indicated by structures in both the competent and incompetent units. Variations and gradations in competency within the folds due to a multi-layered mechanical stratigraphy have led to complex parasitic and disharmonic secondary folds that cause significant departures from the predictions of published models, including the VDDM.

The study area is in the northeastern Brooks Range in the Arctic National Wildlife Refuge of Alaska (Fig. 2). The northeastern Brooks Range exposes many folds that are clearly identifiable as detachment folds (Wallace and Hanks, 1990; Wallace, 1993). The area is well suited for the study of detachment folds because folds in different areas involve the same general stratigraphy in a variety of structural positions and stages of evolution, and because the basal detachment is exposed or can be projected beneath some of the folds.

GEOLOGIC SETTING

The northeastern Brooks Range is the northern extension of the Rocky Mountain fold-and-thrust belt and its stratigraphy is equivalent to that in the subsurface of the Alaskan North Slope petroleum province (Moore *et al.*, 1994). In the northeastern Brooks Range, Paleozoic rocks are divided into two groups that are separated by a sub-Middle Devonian angular unconformity (Fig. 3) (Anderson *et al.*, 1994; Moore *et al.*, 1994). The pre-Middle Devonian rocks, referred to here as 'basement', are a heterogeneous group of multiply deformed and slightly metamorphosed sedimentary and volcanic rocks (Table 1). Late Paleozoic to early Mesozoic rocks above the unconformity are part of a mixed carbonate and clastic sequence formed on a southward-facing passive margin. In the study area, this sequence includes, in ascending order, the Mississippian Kekiktuk Conglomerate, the Mississippian Kayak Shale, the Mississippian and Pennsylvanian Lisburne Limestone, and the clastic Permian and Triassic Sadlerochit Group (Table 1 and Fig. 3).

The dominant structure of the northeastern Brooks Range fold-and-thrust belt is a passive-roof duplex (Banks and Warburton, 1986) that consists of two distinct structural units: (1) a series of northward-displaced, fault-bend folded horses marked by regional anticlinoria and (2) an overlying roof sequence that is deformed into kilometer-scale detachment folds (Namson and Wallace, 1986; Wallace and Hanks, 1990; Wallace, 1993). The unseen floor thrust of the duplex is interpreted to lie within the basement and the roof thrust is within the Kayak Shale. The Kekiktuk Conglomerate has deformed with the basement as part of the horses (Wallace and Hanks, 1990). All of the folds described in this paper are part of the roof sequence of the duplex and are classified as detachment folds because (1) they are defined by a competent unit (Lisburne Limestone), (2) they are cored by an internally deformed incompetent unit (Kayak Shale), and (3) the incompetent unit is detached from and displaced relative to an underlying competent unit (Kekiktuk Conglomerate and basement) (Homza and Wallace, 1995) (Figs 1 & 3). The detachment surface above which the folds have formed has been folded in the regional anticlinoria, which has affected the orientation and, perhaps, the evolution of the detachment folds. The Kayak Shale grades lithologically upward in most locations into a transitional 'lowest Lisburne' (Table 1) unit that is considered here to be part of the competent unit. The Kekiktuk Conglomerate and the basement are referred to collectively here as the 'sub-detachment unit'.

METHODS

In this study, folds were analyzed from four different parts of the northeastern Brooks Range (Figs 2 & 4). Geologic mapping (scale 1:25,000) (Homza, 1993, 1994) has been used to constrain the geometry of each fold in cross-sections normal to plunge, and observations of meso- and microscopic strain indicators have provided evidence to distinguish between fixed- and migrating-hinge mechanisms (e.g. Fischer *et al.*, 1992; Rowan and Kligfield, 1992). We have used the cross-sectional geometry and the strain information, together with the variable detachment depth model, to estimate variations in detachment depth and fold area in order to constrain the evolution of each fold.

Strain indicators and kinematics

Migrating-hinge fold kinematics require that either the synclinal and/or anticlinal hinge move through the

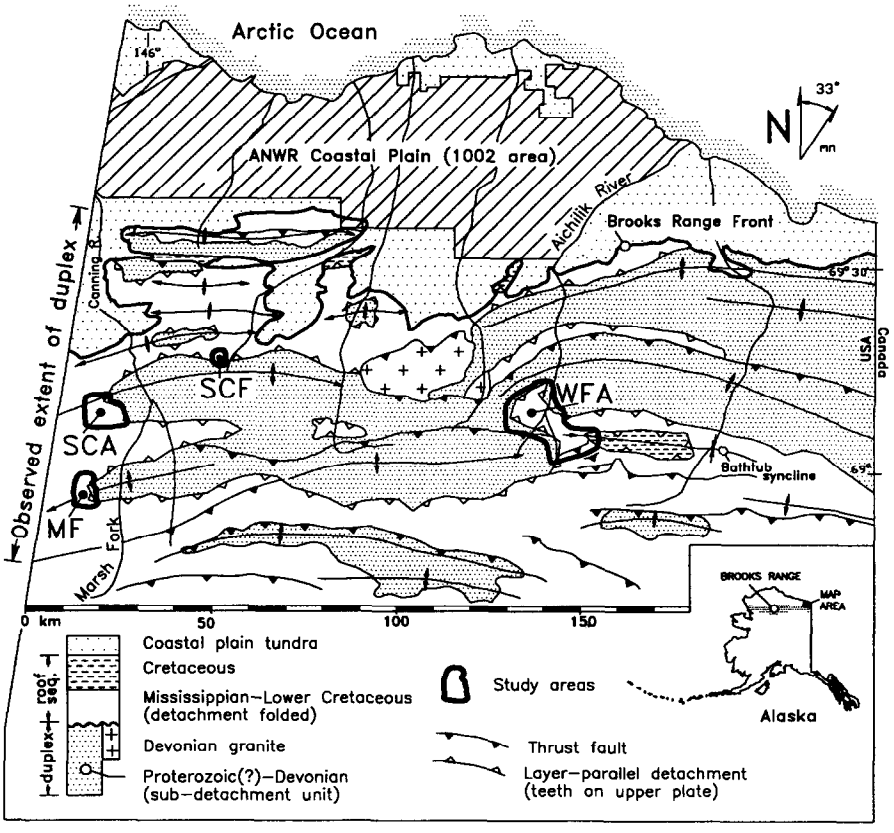

Fig. 2. Simplified structural map of the northeastern Brooks Range and coastal plain of the Arctic National Wildlife Refuge showing the study areas and the regional anticlinoria that mark fault-bend folded horses. SCF = Straight Creek fold, SCA = Salisbury Creek anticline, MF = Marsh Fork transect, WFA = West Fork anticline.

Table 1. Major mechanical-stratigraphic units, and the internal mechanical layering and fold types observed in each

Mechanical-stratigraphic unit (structural position)	Thickness	Lithologic/structural layering	Primary fold structures
Sadlerochit (detached above folds)	Undetermined	Meter-thick beds of shale and siltstone near base, passing upward into 10s of meters of quartz sandstone in decimeter-thick beds. More calcareous to south, siliecous to north.	2nd-order folds (wavelength ~0.1 km) above a secondary detachment at the base of the Sadlerochit. Angular to curved.
Upper Lisburne (primary folded unit)	1200–1600 m	Decimeter-thick laminated wackestone beds in lower part, meter-thick massive grainstone beds in upper part, beds commonly separated by centimeter-thick mudstone horizons and commonly include chert nodules.	1st-order detachment folds (wavelength ~1 km). Angular. Flexural slip along mudstone horizons.
Lowest Lisburne (transitional unit)	100 m	Decimeter-to-meter-thick massive dolomitized wackestone and subordinate grainstone beds interbedded with up to meter-thick shale and mudstone. Shales thicker down section.	2nd-order folds (wavelength ~0.1 km). Angular and parasitic to 1st-order folds. Flexural slip along shale and mudstone layers.
Kayak (detachment unit)	50–1000 m	Shale up to 10s of meters thick, interbedded with thin siltstone, sandstone, and fossiliferous limestone beds. Several ten-meter-thick units of decimeter-thick quartz sandstone beds within thicker shale units in SCA and SCF. Several ten-meter-thick units of decimeter-thick fossiliferous limestone beds within thicker shale units in WFA and MFT.	2nd- and higher-order folds (wavelength ~0.1 km). Disharmonic folds defined by ten-meter-thick competent units within shale. Angular to ptygmatic.
Kekiktuk + basement (sub-detachment unit)	⩾1000 m	Decimeter-to-meter-thick chert-pebble conglomerate and quartz sandstone beds (Kekiktuk). Heterogeneous, bedded-to-massive quartzite, phyllite, chert, metaconglomerate, and minor volcanic rocks (basement).	Folds with ~15 km wavelength define anticlinoria that mark horses in duplex.

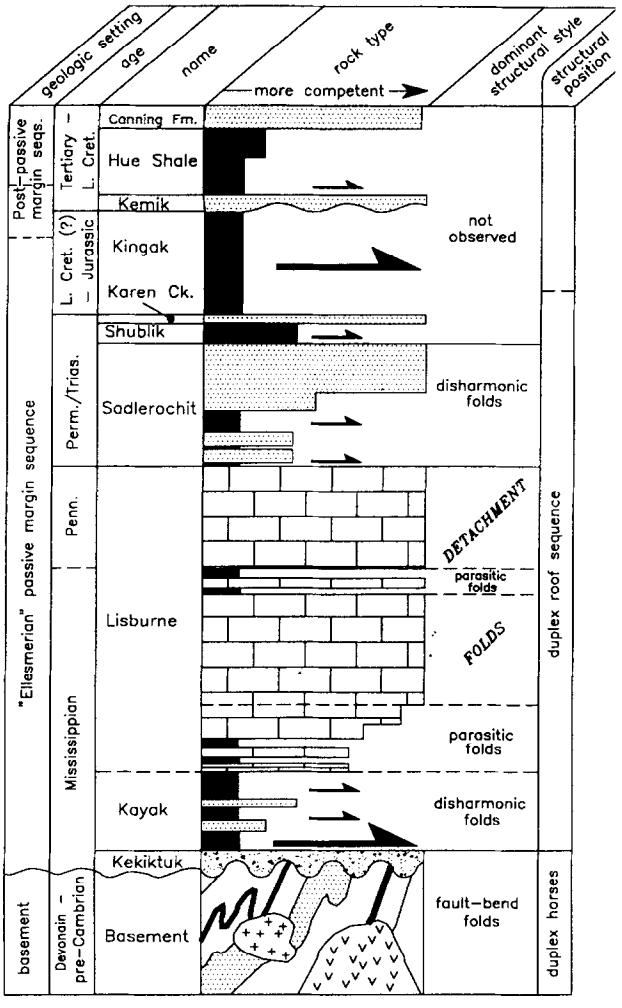

Fig. 3. Generalized column of the mechanical stratigraphy in the northeastern Brooks Range. The lower large arrow indicates the location of the roof thrust of the duplex and the detachment beneath the detachment folds.

competent unit during folding. This suggests that strain indicators that are typical of hinges should be preserved in the fold limbs. For example, if structures typically found in the limbs of flexural-slip folds (e.g. en-echelon tension fractures, orthogonal bedding-normal fractures, and indicators of top-toward the anticline interbed shear (Ramsay and Huber, 1983, 1987; Marshak and Mitra, 1988)) are observed in the fold limbs and they overprint structures typically found in hinges (e.g. intense cleavage, small-scale contractional folds and faults (Ramsay and Huber, 1983, 1987)), then the relationship supports migrating-hinge kinematics. If, however, no such overprinting and no 'hinge structures' are observed in the limbs, then no evidence for hinge-migration kinematics exists. This study utilizes a semi-quantitative strain analysis similar to that used by Fischer *et al.* (1992) to distinguish between fixed- and migrating-hinge kinematics. The analysis consisted of comparing the abundances of common micro-structures in the hinges and in the limbs of folds and noting overprinting relationships (Homza, 1995). These structures include evidence of crystal-plastic deformation (calcite twins, deformation bands), flattened grains, rotated grains, cleavage (spaced and penetrative), stylolites, intra-grain microfractures, and veins. Excellent exposures and access allowed the lowest competent beds to be traversed and sampled across the anticline from syncline to syncline for each fold, which enabled close observation of both mesoscopic structures and overprinting relationships. Figure 5 summarizes the results of observations of strain in 67 thin sections and Fig. 6 graphically shows the distribution of meso- and microscopic strain indicators typically observed in detachment folds in the northeastern Brooks Range.

The variable detachment depth model (VDDM)

The VDDM focuses on the geometry of the incompetent unit and is briefly described here (see Homza and Wallace, 1995 for a detailed explanation). Consider an anticline that formed by plane strain and parallel folding (i.e. constant bed-length and thickness) of a competent unit above an incompetent unit of constant area and with a given undeformed stratigraphic thickness (original detachment depth D_o) (Fig. 7). If the final deformed thickness of the incompetent unit (D_f), as measured beneath the adjacent synclines, equals D_o, then the depth to detachment is the same as before folding and the area of incompetent rock displaced to form the fold (A_o) equals the area uplifted within the fold (A_f). It follows that the shortening (S) required to form the fold multiplied by the original depth (D_o) equals the area uplifted within the fold. This is the basis of the widely accepted 'depth-to-detachment calculation' ($SD_o = A_f$) (Fig. 7b) (Chamberlin, 1910). Most fault-related fold models assume a constant detachment depth (Suppe, 1983; Jamison, 1987; Mitra and Namson, 1989; Dahlstrom, 1990; Mitra, 1990; Suppe and Medwedeff, 1990), which requires a migration of hinges during fold growth (Dahlstrom, 1990; Homza and Wallace, 1995). Although the assumption of a constant detachment depth may be valid for fault-bend and fault-propagation folds, which have rigid ramps, it is not necessarily true for detachment folds, in which internal deformation of an incompetent unit substitutes for a rigid ramp. If it is assumed that $D_o \neq D_f$, then $A_o \neq A_f$, $SD_o \neq A_f$, hinge-migration is not required, and the conventional depth to detachment calculation is invalid, even if total area is conserved (Fig. 7a & c).

The VDDM can be used either in the conventional case, where $D_o = D_f$, or where $D_o \neq D_f$. Thus, it enables evaluation of both fixed- and migrating-hinge folds formed above a detachment unit that may or may not have changed thickness during folding (Fig. 7). For simplicity, the model assumes triangular folds with angular hinges and planar limbs. The model requires a knowledge of D_o and/or D_f (Fig. 7). If either depth is known, then the other can be calculated for any triangular fold geometry using:

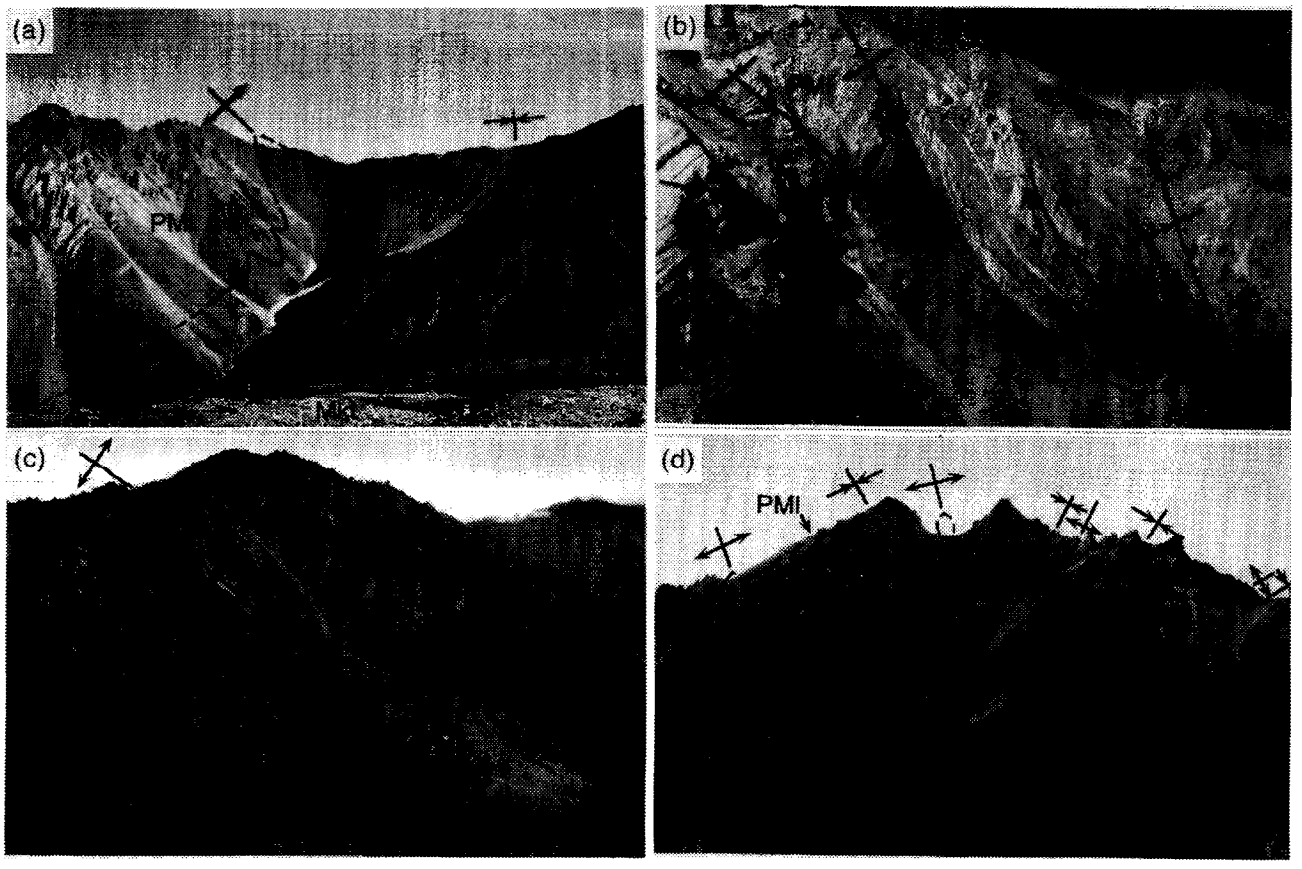

Fig. 4. Photographs of the detachment folds documented in this study. Mkt = Kekiktuk Conglomerate (competent unit below detachment), Mk = Kayak Shale (incompetent unit), PMl = Lisburne Limestone (folded competent unit). (a) Straight Creek fold showing asymmetrical parasitic folds in the lowermost Lisburne, disharmonic folds in sandstone of the Kayak, and near-planar detachment above Kekiktuk (dip slope of light-colored Kekiktuk in foreground projects below darker slopes of Kayak). Distance across photo along base of slope is about 1 km, north is to the left. (b) Salisbury Creek anticline showing thickened Kayak Shale in the core of the fold and near-isoclinal geometry of the Kayak–Lisburne contact at the hinge. Distance across base of photo is about 100 m, north is to the right. (c) West Fork anticline showing parallel fold geometry and thickened Kayak Shale. Distance across the base of the photo is about 1 km, north is to the left. (d) Detachment folds exposed near the southern end of the Marsh Fork transect, including an isoclinal anticline. Kayak has been squeezed out of the core of the anticlines and is significantly thickened below Lisburne. Distance across the base of the photo is about 1.3 km, north is to the right.

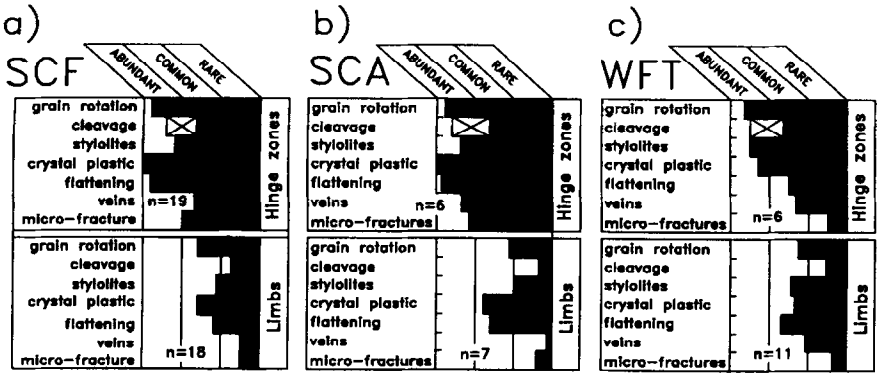

Fig. 5. Histograms showing abundance of strain indicators in thin sections of samples from (a) the Straight Creek fold (SCF), (b) the Salisbury Creek anticline (SCA), and (c) the West Fork transect (WFT). Areas marked with an 'X' indicate the proportion of cleavage that is penetrative.

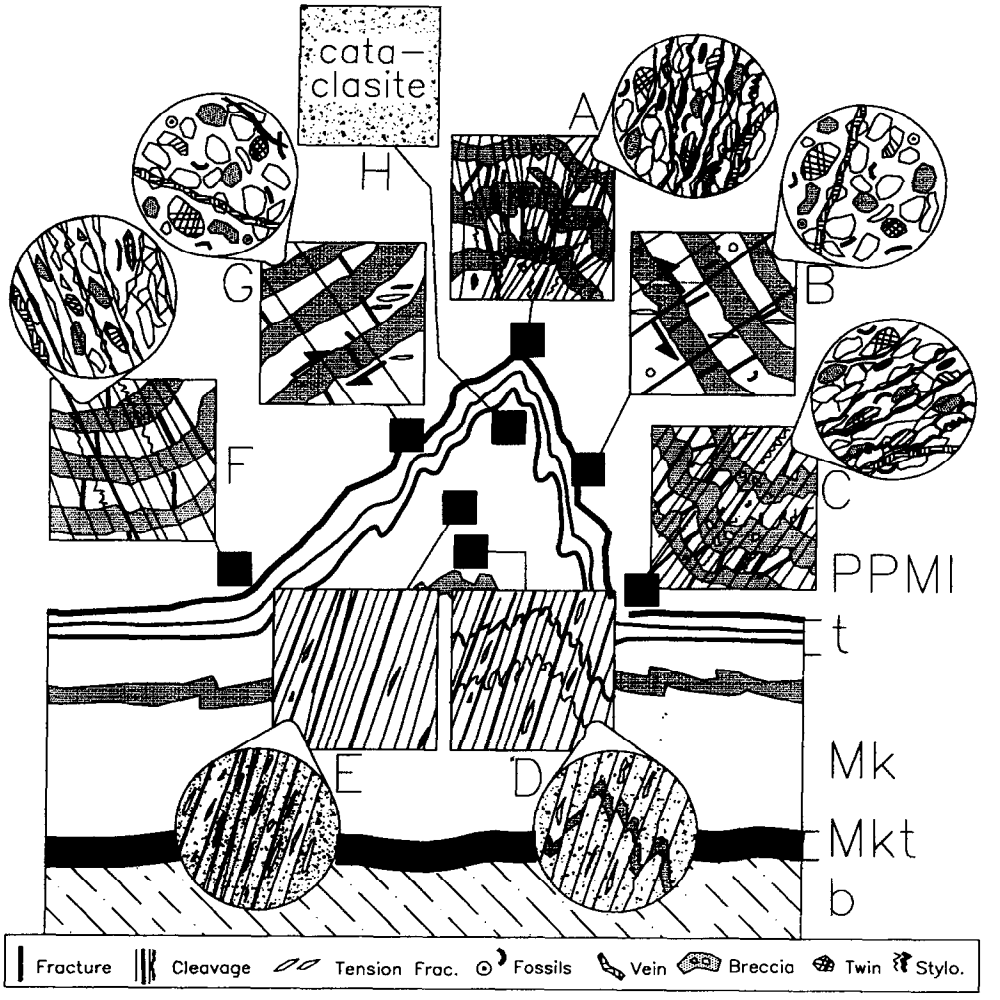

Fig. 6. Schematic diagram illustrating the distribution of strain indicators in a typical detachment fold in the northeastern Brooks Range. Boxes represent about one square meter of rock and circles represent thin sections. The diagram is simplified and the representations of various structures are intended to reflect their existence rather than their detailed characteristics. Note the high strain indicated by the abundance of structures in the hinges in the competent unit (areas A, C, and F) and the solution cleavage and cataclasis in the incompetent unit in the core of the anticline (areas D, E, and H). Contrast these areas with the relatively unstrained limbs (areas B and G). The abundance of veins in areas A and C is under-represented for clarity. Arrows in areas B and G represent bed-parallel shear zones. b = basement rocks (competent), Mkt = Kekiktuk Conglomerate (competent), Mk = Kayak Shale (incompetent), t = mechanically transitional unit, PPMl = Lisburne Limestone (competent).

$$D_f = D_o S/W + D_o - H/2 \quad (3)$$

where W = wavelength and H = height, measured relative to the competent–incompetent contact (Fig. 7) (see Homza and Wallace (1995) for derivations and the use of limb-dip instead of W or H). To simplify discussion, the model incorporates an 'area differential' variable ($A_{\Delta D}$), defined as the difference between the area displaced (A_o) and the area uplifted within the fold (A_f). Alternatively, this can be expressed in terms of depth to reflect changes in structural thickness of the incompetent unit:

$$A_{\Delta D} = W(D_f - D_o). \quad (2)$$

A positive area differential indicates a final depth that is greater than the original depth (Fig. 7c) and a negative area differential indicates a final depth that is less than the original depth (Fig. 7a).

The area beneath a symmetrical or asymmetrical triangular fixed-hinge fold initially increases rapidly, then decreases as the fold tightens beyond an interlimb angle (γ) of 90° (Fig. 8a) (e.g. Wiltschko and Chapple, 1977). According to our model, this initial increase in fold area is accommodated by material moving from beneath synclines into the triangular fold, thereby decreasing both the elevation of the synclines and the $A_{\Delta D}$ value (i.e. $D_f < D_o$). As the fold tightens beyond its maximum area, at $\gamma = 90°$, area is squeezed out of the triangle and moves beneath synclines, which requires either increasing both the synclinal elevation and $A_{\Delta D}$ (i.e. $D_f > D_o$) and/or volume loss in the incompetent unit. Layer-parallel shortening before folding would decrease the amount of required variation in $A_{\Delta D}$ (Fig. 8b). If $A_{\Delta D} = 0$ (i.e. $D_f = D_o$) and no layer-parallel shortening of the competent unit occurs during folding, then the relationship between shortening and uplifted area is linear and hinge

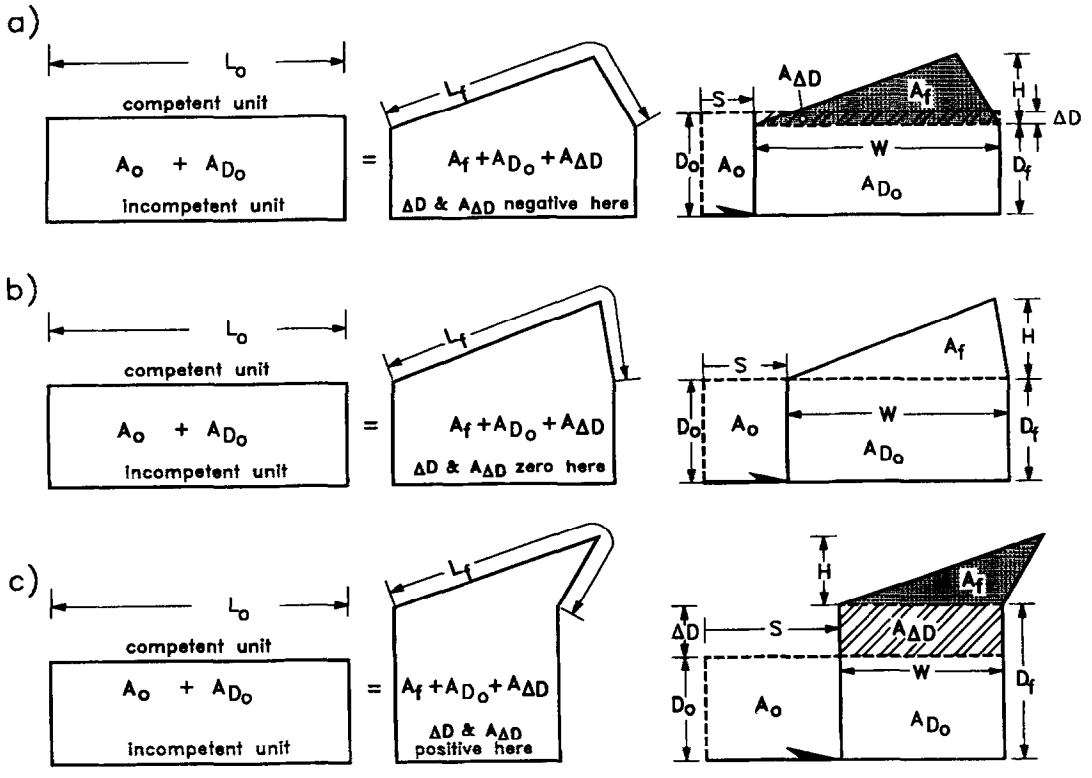

Fig. 7. The variable detachment depth model for detachment folds showing folds formed in an incompetent unit of original thickness D_o. (a) Balanced model of an early-stage fold with small shortening and negative $A_{\Delta D}$. (b) Balanced model of an intermediate-stage fold with $A_{\Delta D}=0$. (c) Balanced model of a late-stage fold with large shortening and positive $A_{\Delta D}$. The original (L_o) and final (L_f) lengths of the contact between the competent and incompetent units are equal. A_{Do} = the total area of incompetent rock minus the displaced area (A_o). $\Delta D=(D_f-D_o)$. Other variables explained in text.

migration is required (Dahlstrom, 1990; Homza and Wallace, 1995). However, layer-parallel shortening of the competent unit during folding could allow detachment depth to remain constant and hinges to remain fixed (e.g. Groshong and Epard, 1994; Epard and Groshong, 1995).

Thus, by comparing natural fold geometries and associated detachment depths to predictions of the VDDM, and taking into account the distribution of strain indicators in both the competent and incompetent units, it is possible to constrain the kinematic path of the fold and to estimate area loss or gain. The distribution of strain in the competent unit provides powerful evidence for differentiating between fixed- vs. migrating-hinge kinematics (Fischer *et al.*, 1992; Rowan and Kligfield, 1992). Comparison of natural fold geometries with the geometric predictions of the VDDM provides an independent means of assessing the applicability of fixed- vs. migrating-hinge kinematics depending on whether detachment depth has varied or remained constant. The primary limitation of the VDDM is that it uses the simplifying assumption that no material moves laterally through the synclines in the plane of section (Fig. 7). The limits imposed by this assumption suggest that the detachment depth variations predicted by the model are maximum estimates.

THE DETACHMENT FOLDS

The areas studied (Fig. 2) include four cross-sectional transects of varying length from different structural positions with respect to the underlying horses. The transects are discussed in order of decreasing interlimb angle, γ, as measured on an enveloping surface on the competent–incompetent contact. Our approach to the geometric analysis and interpretation of the kinematics of the detachment folds is explained in detail using the first transect as an example. For the other folds, only the results of the analysis are presented and discussed.

The Straight Creek fold (SCF)

The Straight Creek fold (Homza, 1993) is an anticline that lies above the north-dipping leading edge of a horse in the central part of the duplex (Figs 2, 4a & 9). Both the sub-detachment unit (basement and Kekiktuk Conglomerate) and the competent–incompetent couplet (Lisburne Limestone and Kayak Shale) that define the detachment fold are well exposed for several kilometers down-plunge. However, the anticlinal hinge of the fold is eroded in the upper part of the competent unit and forms a topographic low along the entire trace of the fold.

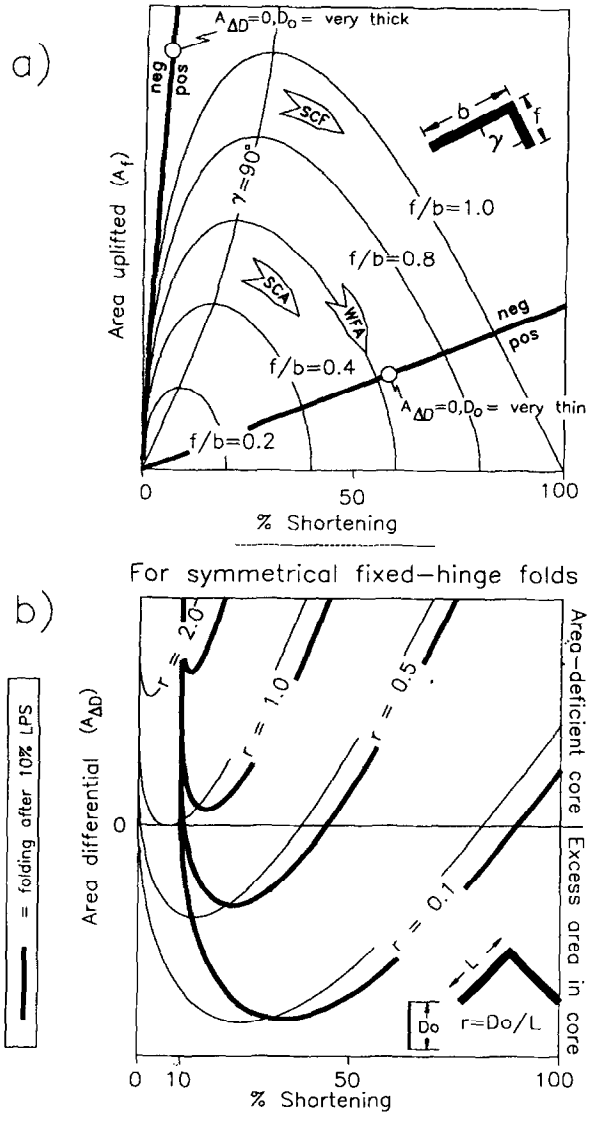

Fig. 8. (a) Graph of uplifted area (A_f) vs percent shortening for folds with varying symmetry and constant total limb length. For a given ratio of forelimb to backlimb length (f/b), maximum A_f is at $\gamma = 90°$, which is reached at low shortening for asymmetrical folds. The two thick lines show examples of paths required for constant-depth folds above either a thick or thin incompetent unit; 'neg' and 'pos' indicate negative and positive values of $A_{\Delta D}$, respectively. Three folds from this study are plotted on the graph. (b) Graph of $A_{\Delta D}$ vs shortening for symmetrical fixed-hinge folds with varying ratios of original depth to limb length ($r = D_o/L$). Folds formed after 10% layer-parallel shortening display a positive shift in $A_{\Delta D}$ values. Separate graphs similar to (b) are required for each ratio of forelimb to backlimb length (f/b). The asymmetrical folds plotted on graph (a) cannot be plotted on graph (b) since it is for symmetrical folds.

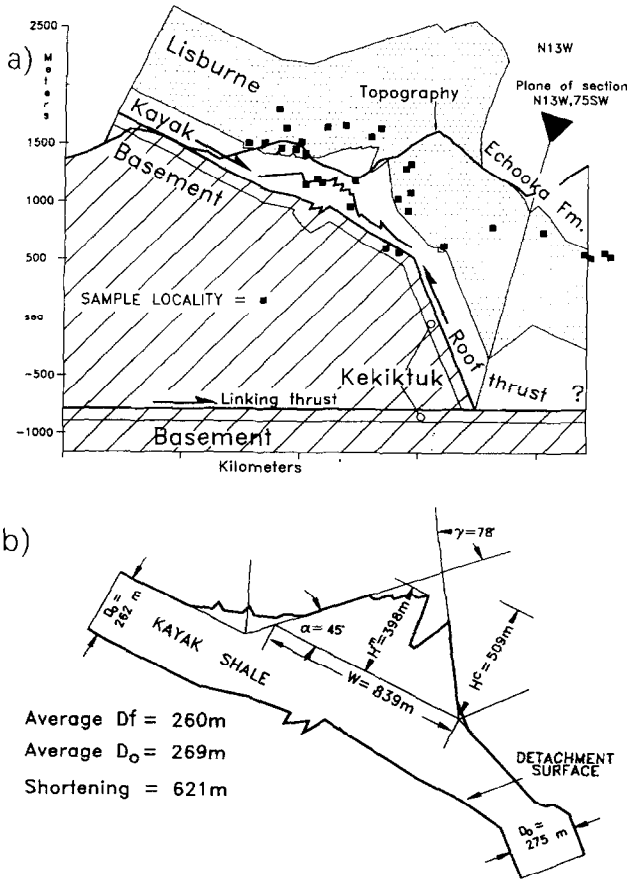

Fig. 9. (a) Balanced cross-section of the Straight Creek fold showing sample localities for strain analyses. (b) The geometry of the Straight Creek fold used to calculate the quantities in Table 2.

Geometry of the Straight Creek fold. The SCF is an open ($\gamma = 78°$), inclined, symmetrical, angular, disharmonic, parallel detachment anticline with a wavelength of 839 m and a height of about 398 m. The fold plunges 15° toward N77°E (Fig. 9; Table 2). The Kayak Shale varies in thickness from about 270 m beneath the synclines to about 650 m in the anticlinal core. Although the axial surface dips almost 60°SE, the SCF is relatively symmetrical and its axial surface is nearly perpendicular to the underlying detachment surface. Parasitic folds in the lowest Lisburne Limestone and disharmonic folds within the Kayak Shale are exposed across the SCF, are most abundant along its axial trace, and have a consistent top-toward-the-anticline asymmetry (Figs 4a & 9).

Strain indicators in the competent folded unit. The abundance of strain indicators is much greater in both primary and parasitic hinge zones than in planar limbs (Figs 5a & 6). In hinge zones in the Lisburne Limestone, penetrative solution cleavage is the most significant deformation mechanism in the finer-grained rocks, whereas intra-grain fracture, calcite twinning, stylolitization, and grain rotation are most important in the coarser-grained rocks. In the limbs, most strain indicators are notably less abundant and penetrative deformation is essentially absent (Figs 5a & 6), except where thin, fine-grained horizons contain minor fault gouge and/or shear-zone fabric that resulted from bed-parallel shear associated with flexural-slip folding. The most abundant features in the limbs are grains rotated toward bedding-perpendicular, flattened grains with long axes perpendicular to bedding, and calcite twins. The bedding-perpendicular orientation of grains around the fold suggests that they were aligned before folding and

Table 2. Geometric variables associated with detachment folds observed in the northeastern Brooks Range

	Observed quantities							Calculated quantities									
								Based on line balance			Based on area balance			Constant depth method		Variable depth method	
Fold	D_o	D_f	H	W	γ	A_f	L_f	S_l	A_o	$A_{\Delta D}$	L_o	S_a	e	Dc	ΔAc	D_v	ΔA_v
SCF	269	260	398	839	78	179,967	1460	621	167,049	−12,918	1480	641	−1.4	290	25,170	254	−5034
SCA	107	115	63	147	40–80	3809	212	65	6955	3146	194	47	9.3	59	−8232	128	1911
WFA	184	184*	738	1084	60	400,674	2154	1070	196,880	−203,794	3262	2178	−34.0	375	207,044	−4	−202,708
unit	m	m	m	m	degs	m^2	m	m	m^2	m^2	m	m	%	m	m^2	m	m^2

D_o = measured undeformed thickness of detachment unit outside the fold (original detachment depth). D_f = measured depth to detachment beneath fold. H = measured fold height. W = measured distance between bounding synclines (wavelength). γ = interlimb angle. A_f = measured fold area beneath competent unit between bounding synclines (including parasitic folds). L_f = measured deformed length of base of competent unit between bounding synclines. S_l = shortening calculated using sinuous bed length ($S_l = L_f - W$). A_o = displaced area, calculated as product of shortening and undeformed thickness of detachment unit ($A_o = S_l D_o$). $A_{\Delta D}$ = area differenfial, difference between displaced area and measured fold area ($A_{\Delta D} = A_o - A_f$). L_o = original bed length calculated using equation (8). S_a = shortening calculated using equation (7). e = extension calculated using equation (9) × 100 for %, extension (+), shortening (−). D_c = constant detachment depth calculated using conventional technique (equation 3). ΔAc = difference between area calculated using conventional technique and observed area ($\Delta Ac = (Dc - D_f)W$). D_v = final depth to detachment beneath fold calculated using equation (5), assuming variable depth. ΔA_v = difference between area calculated using variable−depth technique and observed area ($\Delta A_v (D_v - D_f)W$). * The D_f value for the WFA is not measured beneath the fold, but is projected from the north in the plane of section.

represent bedding-parallel shortening. Limb structures are nowhere observed to overprint hinge structures. Although parasitic folds are common in the lowest Lisburne Limestone in the primary anticlinal hinge zone, the limbs of these folds contain no penetrative fabrics and many fewer strain indicators than do their hinges. Hinge deformation is observed in the upper, more competent part of the Lisburne Limestone only in the northern syncline in the form of the penetrative cleavage. A similar high-strain zone in the Lisburne in at least the lower part of the anticlinal hinge may have been preferentially eroded.

Strain indicators in the incompetent unit. Two 10 m thick competent quartz sandstone layers within the Kayak Shale lie between thicker, less competent shale intervals and define complex disharmonic folds in the lower part of the core of the SCF (Figs 4a & 9). Some of these folds are associated with 'into-the-plane' thrust faults (i.e. with displacements sub-parallel to the fold trend) and they are tightest (in some cases isoclinal) along the lower boundary of the sandstone layers. Intra-grain microfractures, quartz veins, deformation lamellae, flattened grains, and spaced cleavage are abundant in the hinges of these folds. In contrast, the limbs contain many fewer veins, no visible cleavage, and rounder, less fractured grains with more uniform extinction.

Shale in the Kayak in the cores of both the SCF and the tight intra-formational disharmonic folds displays a penetrative solution cleavage that has transposed bedding. In the cores of some tight folds, the shale is either reduced to a siliceous gouge or it is completely removed and the fold is truly isoclinal. Pencil cleavage is common in more open cores. Beneath the planar limbs of both the SCF and the disharmonic folds, the Kayak Shale is fissile with a spaced cleavage sub-parallel to bedding. Centimeter- to meter-scale fold trains in the Kayak Shale both in the hindward synclinal hinge and adjacent to the forward synclinal hinge display top-toward-the-anticline asymmety consistent with flow from beneath the syncline into the anticlinal core of the fold.

Geometric analysis and kinematic interpretation of the Straight Creek fold. Qualitative indications of layer-parallel shortening before folding suggest that regardless of how the incipient Straight Creek fold formed, beds were first shortened and thickened to some degree. The distribution of penetrative deformation in the hinges of the primary anticline, the parasitic folds in the lowest Lisburne, and the disharmonic folds in the Kayak, together with the lack of hinge structures overprinted by limb structures, suggests folding with fixed hinges and rotating limbs.

Analysis of the fold geometry with both the standard constant depth-to-detachment method (e.g. Chamberlin, 1910; Jamison, 1987; Mitra and Namson, 1989) and the VDDM suggests detachment depth changes consistent with fixed-hinge kinematics. The quantities used and derived in these analyses are given in Table 2. First, we consider the standard calculation where Dc is the calculated constant detachment depth, A_f is the measured fold area, and the displaced area (A_o) is assumed to equal A_f (Fig. 10a):

$$Dc = A_f / S$$
$$Dc = 179,967\ m^2 / 621\ m = 290\ m. \quad (3)$$

When this solution is compared with the depth to detachment measured beneath the fold (D_f = 260 m), it is found to be greater than the measured detachment depth by 30 m. Further, if we multiply the calculated depth by the fold wavelength (839 m), the calculation suggests that about 25,000 m^2 more incompetent material should be present beneath the fold than can be accounted for (Fig. 10a; ΔAc, Table 2).

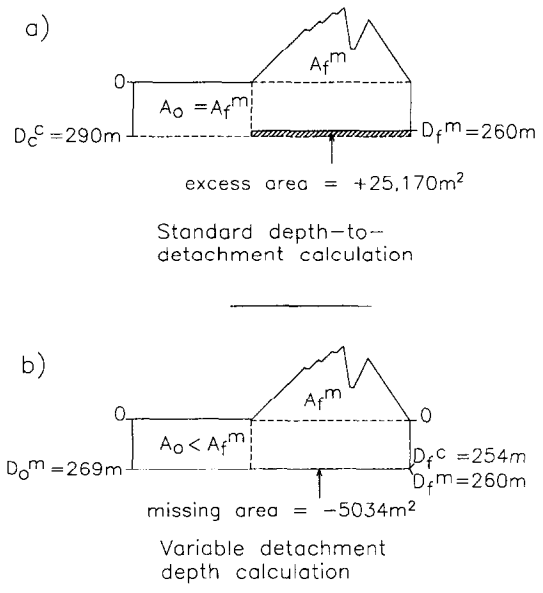

Fig. 10. Diagram showing the difference between the standard technique for calculating depth to detachment and the variable detachment depth method as applied to the Straight Creek fold. (a) The standard method uses equation (3) to determine a constant detachment depth (D_o) of 290 m. This calculation over-estimates incompetent unit area by approximately 25,000 m^2 and detachment depth by 30 m. (b) The variable detachment depth method uses equation (6) to calculate a variable 'instantaneous' detachment depth of 254 m. This method under-estimates incompetent unit area by approximately 5000 m^2 and detachment depth by 6 m.

The variable detachment depth method does not assume that $Ao = A_f$. To use the VDDM, we first take the measured undeformed stratigraphic thickness of the Kayak Shale (269 m) as the measured original detachment depth (D_o) to calculate the area differential:

$$A_{\Delta D} = SDo - A_f$$
$$A_{\Delta D} = 167,049\ \text{m}^2 - 179,967\ \text{m}^2 = -12,918\ \text{m}^2. \quad (4)$$

Then, we solve for the calculated final detachment depth beneath the fold (D_v) using equation (2):

$$D_v = A_{\Delta D}/W + D_o$$
$$D_v = (-12918\ \text{m}^2/839\ \text{m}) + 269\ \text{m} = 254\ \text{m}. \quad (5)$$

When this solution is compared with the measured depth to detachment, it is found to be less than the measured detachment depth by 6 m. If we multiply the calculated depth by the fold wavelength (839 m), the calculation suggests that about 5000 m^2 less incompetent material should be present than is accounted for beneath the fold (Fig. 10b; ΔA_v, Table 2). This number is a minimum because the calculations do not account for loss of area by solution cleavage, as is observed in the fold core. This area discrepancy could represent errors resulting from imprecise measurements. However, thrust faults in the fold core indicate material transport into the plane of section and suggest that the area disparity may reflect and quantify such non-plane strain.

Up to this point, our analysis has assumed constant bed length and thickness (parallel folding) in the competent unit. However, Groshong and Epard (1994) and Epard and Groshong (1995) have pointed out that bed-parallel shortening in the competent unit may contribute to detachment fold growth and can be accommodated by penetrative strain and structures too small to show on a cross-section. Our observations suggest that at least minor bed-parallel shortening has occurred in the competent unit, but they are not sufficiently detailed to allow us to quantify that shortening directly. However, we can estimate apparent bed-parallel shortening of the competent unit by comparing observed deformed bed length (L_f) with original bed length (L_o) determined from area balance of the incompetent unit (Fig. 7). Shortening is determined from competent bed length using:

$$S = L_o - W. \quad (6)$$

The value of shortening we have used so far (S_l) has been calculated using deformed bed length based on the assumption that $L_f = L_o$. However, using quantities from Table 2, we can calculate a different estimate of shortening (S_a) by assuming that the incompetent unit has constant cross-sectional area before and after deformation:

$$D_o(S_a + W) = A_f + WD_f$$
$$S_a = (A_f + WD_f)/D_o - W \quad (7)$$
$$S_a = (179,967\ \text{m}^2 + (839\ \text{m} \times 260\ \text{m}))/269\ \text{m} - 839\ \text{m}$$
$$= 641\ \text{m}.$$

S_a can then be inserted in equation (6) to calculate a value of L_o that is not derived from the measured deformed bed length, L_f (Table 2):

$$L_o = S_a - W$$
$$L_o = 641\ \text{m} + 839\ \text{m} = 1480\ \text{m}. \quad (8)$$

Finally, values of apparent extension (e) can be calculated using L_o and L_f (Table 2):

$$e = L_f/L_o - 1$$
$$e = 1460/1480 - 1 = -0.01. \quad (9)$$

This approach provides an estimate of about 1% layer-parallel shortening of the base of the competent unit. This is consistent with our initial assumption of parallel folding in the competent unit, although it does not account for the possibility of loss of cross-sectional area in the incompetent unit.

For the Straight Creek fold, the VDDM provides a better fit to the observations than does the conventional depth-to-detachment calculation. The differences are small and could be attributed to minor discrepancies between the actual and reconstructed fold geometries. Despite this possibility, the Straight Creek fold can serve as an example to show how the VDDM can be used to analyze fold kinematics. The geometric solution suggests that the detachment depth effectively decreased during folding from 269 m to 260 m as material moved from the synclines into the anticlinal core, as would be expected in fixed-hinge folding (e.g. Wiltschko and Chapple, 1977). The asymmetry of disharmonic folds in the Kayak is

consistent with such motion. The general location of the SCF on Fig. 8(a & b) (≈35% shortening) suggests that, when fold growth ceased, the area differential, although still negative, was approaching zero (i.e. detachment depth was increasing, and thus, was once less than the current depth). Since solution cleavage indicates area loss in the fold core, the detachment depth would likely increase at a slower rate than indicated on the idealized constant-area graphs of Fig. 8.

Thus, considering both the geometric modeling of the SCF and the distribution of strain indicators within it, we hypothesize that (1) early layer-parallel shortening is recorded in the limbs, (2) the uplifted area initially increased rapidly (Fig. 8) as fold limbs rotated about both the primary and parasitic hinges, which were fixed with respect to the rock, (3) the distance between the synclines and the detachment (detachment depth) decreased by at least 9 m (from D_o to D_f) as the limbs rotated and material moved into the anticlinal core, and (4) further limb rotation resulted in a decrease in uplifted area, which promoted area loss by penetrative solution cleavage in the core, perhaps coupled with a minor increase in detachment depth (from Fig. 8). Even with area loss due to solution cleavage, a net area gain is still apparent in the core of the SCF, suggesting non-plane strain, which is supported by into-the-plane thrust faults in the lower anticlinal core.

The Salisbury Creek anticline (SCA)

The Salisbury Creek transect lies above the same fault-bend folded horse as the Straight Creek fold but is about 35 km southwest of the SCF and structurally overlies the gently dipping backlimb of the horse (Figs 2 & 11). The form surfaces of the sub-detachment unit, the incompetent unit, and the competent unit together describe a series of north-vergent to upright and symmetrical detachment folds. One particularly well-exposed north-vergent anticline, the Salisbury Creek anticline (SCA) (Figs 4b & 11) (Homza, 1994; Homza and Wallace, 1995), is discussed in detail below.

Geometry of the Salisbury Creek anticline. At the Lisburne–Kayak contact, the Salisbury Creek anticline is an open to tight, inclined, northward asymmetric, angular, disharmonic, parallel detachment fold with a wavelength of 147 m, a height of 63 m, and a slight westward plunge. The fold can be traced for 20 km down plunge where, up-structural section, it increases in height, wavelength, and interlimb angle. The fold interlimb angle is about 40° at the hinge on the Kayak–Lisburne contact, but this angle increases to about 80° both up- and down-structural section. The change in dip of the contact down section defines gentle secondary synclines on the limbs of the anticline (Figs 4b & 11b). A train of smaller detachment folds lies immediately hindward of the SCA at the Kayak–Lisburne contact.

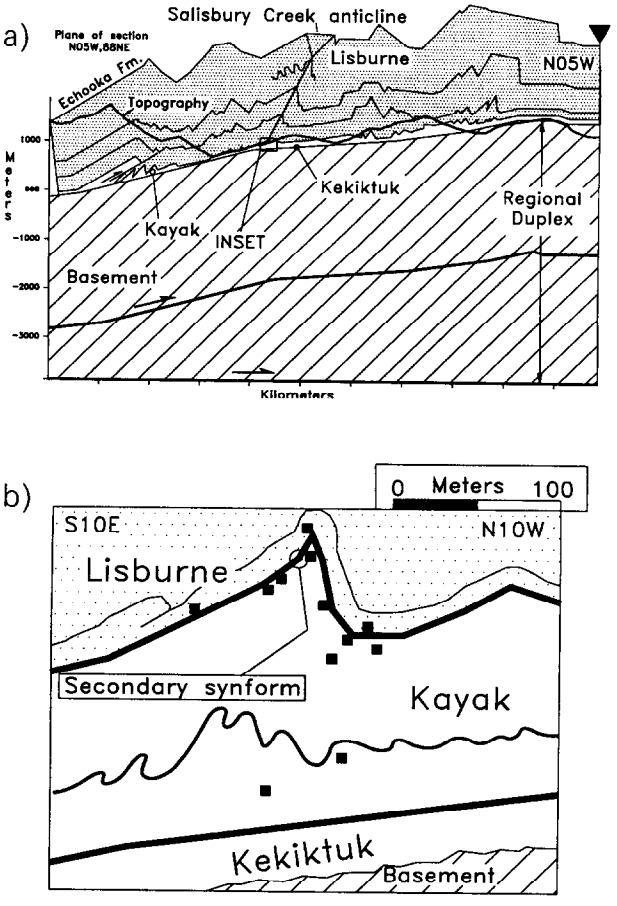

Fig. 11. (a) Balanced cross-section of the Salisbury Creek transect. (b) Detail of the Salisbury Creek anticline showing sample localities for strain analyses.

Strain indicators in the competent folded unit. Five parasitic folds that are exposed in the upper Lisburne where it contains alternating competent–incompetent layers are out of phase with the fold train at the Kayak–Lisburne contact (Figs 3 & 11a). These upper parasitic folds are about 5 km off the section line and so are shown only as representative of the structure of the upper Lisburne. Beds in the Lisburne above and below these folds are relatively straight, indicating that these parasitic folds are detached from adjacent layers. Many minor thrust faults and folds are exposed in the synclinal and anticlinal hinges at the Kayak–Lisburne contact, and well-developed calcite-filled veins, solution cleavage, and stylolites are associated with them (Figs 5b & 6). Although the forelimb is more deformed than the backlimb, no evidence was observed that limb structures overprinted hinge structures in either limb. A single thrust fault with less than 10 m of displacement duplicates part of the lowest Lisburne in the backlimb (Figs 4b & 11b).

Strain indicators in the incompetent unit. As in the Straight Creek fold, disharmonic folds in several meter-thick competent sandstone beds within the Kayak display top-toward-the-anticline asymmetry consistent

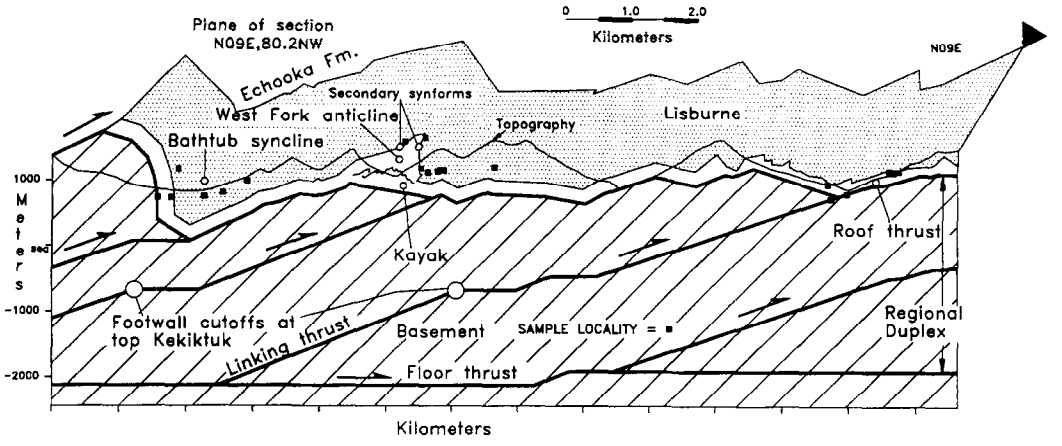

Fig. 12. (a) Balanced cross-section of the West Fork transect showing sample localities for strain analyses.

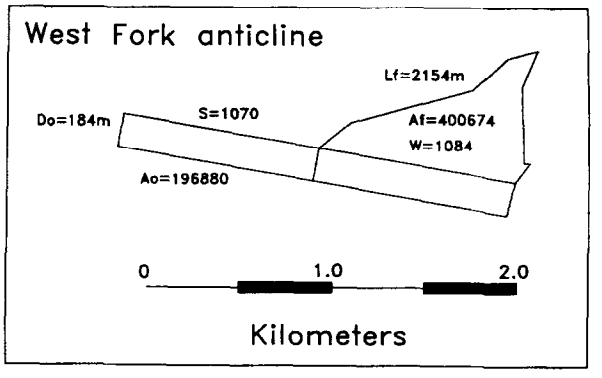

Fig. 12. (b) The geometry of the West Fork anticline used to calculate the quantities in Table 2.

with transport of material into the anticlinal core. Strain in the detachment unit visibly increases toward the hinge of the anticline, where the tightest disharmonic folds are developed in the sandstone beds and where shale layers display both crenulation cleavage and solution cleavage. A siliceous gouge-like cataclasite is exposed in the uppermost Kayak, where the fold is tightest in the core of the SCA.

Geometric analysis and kinematic interpretation of the Salisbury Creek anticline. For the SCA, the variable depth equations (equations 4 and 5) result in closer matches between observed and calculated depths and uplifted areas than does the constant depth equation (equation 3) (Table 2). The observed difference between the original stratigraphic thickness of the detachment unit and the final detachment depth indicates that the synclines were elevated by about 8 m (positive $A_{\Delta D}$). An apparent net area loss of 1911 m^2 in the incompetent core of the fold (ΔA_v, Table 2) is supported by strong solution cleavage and cataclasite development where the fold is tightest in its core near the Kayak–Lisburne contact. The calculated value of apparent extension of the base of the competent unit (e, Table 2) suggests a layer-parallel extension of about 9%, which is not consistent with the observed evidence for at least minor shortening within the limbs. However, the calculation could also yield this result if the incompetent unit lost area, as we suggest. The strong hinge deformation, lack of overprinted hinge structures on the limbs, and top-toward-the-anticline asymmetry in the Kayak suggest fixed-hinge kinematics for the SCA. The change in detachment depth indicated by the VDDM better fits the geometry of the SCA than does a model that assumes constant depth and migrating hinges. Thus, the SCA is interpreted as a fixed-hinge detachment fold formed with limb rotation, area loss, an increase in detachment depth, and minor thrust faulting in the backlimb.

The West Fork anticline (WFA)

The West Fork transect crosses the central part of the fold-and-thrust belt along the west fork of the Aichilik River (Fig. 2). The transect includes multiple detachment folds above at least three horses (Fig. 12). In this region, the lowest Lisburne is very rich in chert and has nearly no fine-grained carbonate component. Thus, the competent–incompetent contact is sharp here, rather than gradational as it is in the other transects.

Linking thrusts in the regional duplex are apparently more closely spaced here than in the other transect areas. Just to the south of and to the west of the West Fork transect, thrusts are observed to cut up-section from the basement and through the forelimbs of detachment folds in the roof sequence (Homza, 1992). Thus, folds in the roof sequence are closely associated with thrust faults in the basement along this transect. However, the folds in the roof sequence are clearly detachment folds since the Kayak Shale is thickened in the core of each fold (Fig. 12), whereas fault-bend and fault-propagation folds involving both the Kayak and the Lisburne are apparently absent. Here, most detachment folds are open to tight, angular, and north-vergent. We focus our analysis on the West Fork anticline (WFA) (Figs 4c & 12), a large anticline that is exposed along strike for over 13 km in the

central part of the transect and is truncated up-plunge by a linking fault in the duplex.

Geometry of the West Fork anticline (WFA). The WFA and its adjacent forward syncline (Figs 4c & 12) are close ($\gamma \approx 60°$), inclined, northward asymmetric, angular, parallel folds that plunge 10° toward S81°E. The WFA contains only a few small parasitic folds, hence its geometry is nearly triangular. As with anticlines in each of the transect areas, the hinge of the WFA is preferentially eroded in many areas. The fold is tightest in the hinge at the Kayak–Lisburne contact and this local increase in tightness introduces gentle, secondary synclines up-structural section in the limbs of the anticline. However, down-plunge exposures show that, like the SCA, the interlimb angle of the WFA increases up-section and parasitic folds are present within the upper Lisburne off the line of cross-section.

The base of the Kayak is not exposed beneath the WFA and its position is interpreted based on observations along the line of section immediately north and south of the fold (Fig. 12a). The Kayak Shale is interpreted to be 725 m thick in the core of the anticline and is observed to be 184 m thick where it is relatively undeformed beneath straight panels of Lisburne 2 km to the north.

Strain indicators in the competent folded unit. Mesoscopic contractional faults and tight folds are abundant along the Kayak–Lisburne contact in the hinge of the WFA but are absent in the limbs. Mesoscopic and limited microscopic samples show that strain indicators are concentrated in fold hinges along the West Fork transect and that grain rotation and cleavage are the most abundant observed deformation mechanisms (Figs 5c & 6). Again, the most common features in the limbs are stylolites, flattened grains, and rotated grains, all of which may be associated with layer-parallel strain prior to folding since they are perpendicular to bedding around the fold. Interbed slip surfaces are apparent in the limbs in the Lisburne. As with all of the other transect areas, penetrative cleavage is much more common in hinges than in limbs and represents the most common microscopic expression of shortening in the lowest Lisburne.

Strain indicators in the detachment unit. Several meter-thick competent limestone beds lie within the Kayak Shale along this transect. In the core of the WFA, these beds are tightly folded and offset along south-dipping thrust faults with meter-scale displacements. Strain in the shale component of the Kayak in the core of the WFA is dominated by penetrative solution cleavage that has transposed bedding.

Geometric analysis and kinematic interpretation of the West Fork anticline. The West Fork anticline has a relatively simple geometry, but one that requires complex kinematics to account for its excess area. The linking fault that defines the leading edge of a horse in the underlying duplex truncates the forelimb up-plunge, but it is interpreted to lie directly beneath the fold on the line of section (Fig. 12a). This strongly suggests that folding was a response, at least in part, to horse emplacement, so the conventional assumption of detachment fold formation above a planar detachment is not applicable. The base of the Kayak, which is observed to be the detachment along the other transects, is not observed here, so we must estimate its position and geometry. The variable depth model may be applied in order to determine the area that must be accounted for and to constrain a kinematic model that incorporates this area and the role of horse emplacement.

If a constant detachment depth is assumed for the WFA, then either a detachment depth of 375 m is calculated using the measured fold area (equation 3) or the fold includes an excess uplifted area ($A_{\Delta D}$) of about 203,794 m^2 if the known stratigraphic thickness ($D_o = 184$ m) is assumed to be the constant detachment depth (Table 2). When the known D_o value and the area differential are used with the VDDM (equations 4 and 5), the final detachment depth beneath the fold is calculated to be 4 m above the base of the competent unit in the synclines, which is an obviously unrealistic result. Exposures in the plane of section north of the fold suggest a projected depth to detachment of at least 184 m (Fig. 12).

With this depth, the WFA presents a problem because about half of the area uplifted within the fold cannot be accounted for given the observed fold shortening. However, this extra area could be accounted for by one of several models. The first involves 'bulldozing' of the Kayak Shale along the sub-fold thrust in front of the basement horse (Fig. 12a). Excess area would be pushed into place beneath the fold by an excess of shortening in the basement and Kayak Shale relative to the overlying Lisburne. This excess shortening could have been taken up in the Lisburne north and/or south of the area of the section by forward and/or hindward displacement, respectively, of the Lisburne relative to the Kayak Shale.

The second model would account for the excess incompetent rock by its transport from out of the plane of section. Such non-plane strain is commonly associated with folds that have a significant plunge, as does the WFA.

The third model invokes inversion of a local extensional basin formed during Middle Devonian to Mississippian rifting (Anderson *et al.*, 1994) and filled with an anomalous thickness of Kayak Shale. This basin would be preferentially inverted along the observed thrust fault during Cenozoic shortening and the excess basinal thickness would become excess uplifted area in the WFA. In effect, this model suggests that an original detachment depth of 184 m beneath the fold is too shallow and instead an inclined detachment is required at a depth of at least 375 m beneath the synclines.

Thickness changes in the Kayak and underlying Kekiktuk near the WFA do not appear to be sufficiently large or abrupt to support this model (LePain, 1993; LePain *et al.*, 1994).

For each of these models, the VDDM allows the excess area to be calculated, depending upon which original depth is selected. The observations and the cross-section, as drawn (Fig. 12a), permit any of the three models.

The calculated value of apparent extension of the base of the competent unit (*e*, Table 2) suggests layer-parallel shortening of about 34%. However, the field and microscopic observations (Figs 4c & 5c) do not indicate significantly more small-scale to penetrative shortening in the limbs of the WFA than in the SCF and SCA, as would be expected. The large calculated value of apparent extension probably reflects mainly the large increase in area of the incompetent unit, with only a partial contribution from layer-parallel shortening of the competent unit.

The Marsh Fork transect (MFT)

The Marsh Fork transect includes impressive exposures above the crest and gently dipping forelimb of the southernmost horse in the duplex (Figs 2, 4d & 13). The form surface of the sub-detachment unit, the entire Kayak Shale, the Kayak–Lisburne contact, and the lowest Lisburne Limestone are each very well exposed in the area.

Geometry of the Marsh Fork transect. Along this transect, two primary anticlines are separated by a planar panel that parallels the underlying detachment. The two anticlines are each composed of a train of smaller detachment folds at the Kayak–Lisburne contact whose hinges coalesce up-section into a single large fold in the upper Lisburne Limestone (Fig. 13). The thickness of the Kayak Shale varies from about 290 m beneath the straight panel to in excess of 700 m in some anticlinal cores. The detachment fold trains include open to isoclinal (tightest at the Kayak–Lisburne contact in anticlinal hinges), upright to inclined, disharmonic, parallel, and mostly angular folds (Figs 4d & 13). The hinges of the tightest anticlines consistently form topographic lows due to preferential erosion where strain is greatest.

Strain indicators along the Marsh Fork transect. In the lowest Lisburne Limestone, mesoscopic strain indicators are concentrated in the hinges of all observed folds. The most common strain indicators are penetrative cleavage, tectonic breccia, veins, and minor folds and faults. Strain indicators are more common in the limbs of tighter folds than in the limbs of more open folds. Minor thrust faults ($\leq$5 m displacement) were seen exclusively in hinge zones.

Strain indicators in the Kayak Shale are also concentrated in the hinge zones and the intensity of strain corresponds roughly with the tightness of the overlying fold in the Lisburne Limestone. Kayak in the hinges of more open detachment folds typically contains open-to-close disharmonic folds and relatively less penetrative axial planar cleavage than Kayak beneath isoclines. Beneath isoclinal anticlines, the uppermost Kayak is typically a mixed carbonaceous–siliceous, gouge-like cataclasite. These cataclasites are associated both with shale that displays transposed laminations parallel to penetrative cleavage and with various forms of silica and carbonate mineralization. All of these features beneath isoclinal anticlines suggest fluid migration in the Kayak.

As with folds in the other transects, fold trains defined by competent horizons within the Kayak display top-toward-the-anticline asymmetry that is consistent with transport of material toward the anticlinal core. The undeformed thickness of the Kayak is typically less than 250 m in the northeastern Brooks Range (Imm *et al.*, 1993, Homza, unpublished field data), about 40 m less than the thinnest Kayak exposed along the transect. Since even the thinnest section of Kayak along the transect displays structural thickening by folding, thrusting, and internal deformation, we conclude that the Kayak Shale has been structurally thickened everywhere along this transect (Figs 4d & 13).

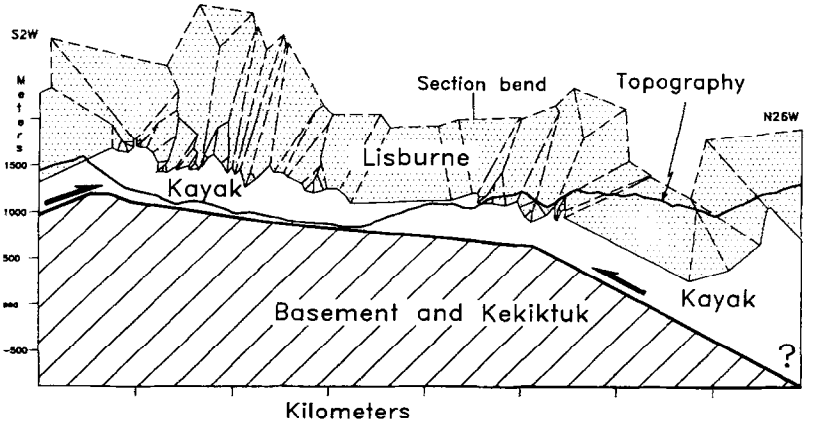

Fig. 13. Cross-section of the Marsh Fork transect.

Kinematic interpretation of the Marsh Fork transect. The complex geometry and abundance of parasitic folds along the Marsh Fork transect preclude simple geometric modeling. However, the observations of geometry and mesoscopic strain along the transect indicate that the incompetent unit did not maintain constant thickness during deformation. Rather, it was significantly thickened beneath anticlines, synclines, and detachment-parallel panels, which indicates that a constant-depth model does not apply to these folds. The distribution of mesoscopic structures suggests that hinges were fixed during folding and that incompetent rock flowed toward anticlinal cores. Thus, we suggest that the major detachment anticlines in the competent unit formed as composites of chevron-like parasitic folds. These folds were accommodated in the incompetent unit by thickening and possible area loss manifested by solution cleavage and recrystallization in tight fold cores. Since the lowest Kayak is dramatically shortened directly above generally flat and undeformed beds of Kekiktuk, we suggest that the stratigraphic position of the detachment remained near the base of the Kayak Shale throughout deformation.

THE ROLE OF MECHANICAL STRATIGRAPHY IN THE GEOMETRY OF DETACHMENT FOLDS

In the northeastern Brooks Range, the contact between the incompetent unit (Kayak Shale) and the competent unit (Lisburne Limestone) is commonly sedimentologically (LePain, 1993) and mechanically gradational (Fig. 3). The top of the Kayak is typically defined by the uppermost meter-thick, fissile, black shale interval. However, structurally weak shales persist into the lowest Lisburne, which is primarily composed of decimeter-thick carbonate beds. Higher in the Lisburne, the shales are effectively absent and the carbonate beds of the upper Lisburne are meters thick and very massive. This stratigraphy results in an upward gradation in structural style from penetrative fabrics and small-scale faults and folds in the lowest, finest-grained rocks, to parasitic flexural-slip folds in the transitional strata, to primary flexural-slip folds in the upper part of the competent unit.

Such stratigraphic variations are common in the rocks of fold-and-thrust belts and define multilayer mechanical stratigraphies that display consequent variations and gradations in structure within detachment folds. Increasing competent bed thickness and abundance in a multilayer stratigraphy leads to folds with greater arc wavelength and interlimb angle, whereas decreasing bed thickness, grain size, and strength due to rock composition lead to increasing importance of small-scale structures and penetrative strain (e.g. Currie *et al.*, 1962; Ramsay, 1974; Ramsay and Huber, 1987). Most geometric approaches, including the analytical approach used in this paper (the VDDM), assume simple geometries and sharp boundaries in competency and do not address structures in the competent unit that are too small to show on a cross-section. Such approaches cannot fully describe folds that involve complex stratigraphically controlled variations in geometry and kinematics.

APPLICABILITY OF DIFFERENT APPROACHES TO THE ANALYSIS OF NATURAL DETACHMENT FOLDS

The analytical approach we present (VDDM) is based primarily on the assumptions of constant cross-sectional area and competent bed length. This approach encompasses most previous models for detachment folds but, unlike them, is not limited by the assumption that detachment depth remains constant. Poblet and McClay (1996) have taken a similar approach to ours and explored its implications for four specific geometric-kinematic models for detachment folds and for variation of forelimb thickness with fixed hinges or variable layer-parallel shear.

Groshong and Epard (1994) and Epard and Groshong (1995) have pointed out that layer-parallel shortening in the competent unit may play an important role in the growth of detachment folds, and hence that the assumption of constant competent bed length may not be valid in some cases. They have proposed a method that uses fold geometry to take into account complex variations in competency and to quantify layer-parallel shortening throughout a detachment fold. Like most previous models for detachment folds, their approach is based on the assumptions of constant cross-sectional area and detachment depth. Despite the fact that their method addresses layer-parallel shortening in the competent unit, we have chosen not to use it because it depends on the fundamental assumption that detachment depth remains constant, an assumption that our observations and those of others (Wiltschko and Chapple, 1977) have shown to be invalid for at least some natural detachment folds.

The focus of our analysis has been on whether or not detachment depth remains constant and fold hinges migrate. The approach we outline in this paper provides a useful way to analyze the relationships among cross-sectional area, competent bed length, shortening, and detachment depth. We obtain results that are more consistent with our observations of natural folds if we assume that detachment depth varies rather than remaining constant. Thinning or thickening of the incompetent unit accounts for the observed differences between detachment depth and original stratigraphic thickness as well as accounting for the changes in fold area predicted if hinges are fixed, as our observations suggest. Although constant bed length and thickness in the competent unit are used as a simplifying assumption in our analysis, area discrepancies and calculation of apparent layer-parallel shortening of the base of the

competent unit provide some insights into the magnitude of strain in both the competent and incompetent units.

Our analysis is inconclusive about the role of layer-parallel shortening of the competent unit in the detachment folds we have observed. The small-scale structures and strain observed in fold limbs indicate that some layer-parallel shortening has occurred in the competent unit, although we suggest that this largely or entirely preceded folding. In the incompetent unit, loss or gain of cross-sectional area may have accompanied layer-parallel shortening in the competent unit.

Our approach assumes constant competent bed length and the approach of Groshong and Epard (1994) and Epard and Groshong (1995) assumes constant detachment depth. The advantages of both methods might be realized if these assumptions could both be eliminated. The VDDM can easily be adapted to account for layer-parallel shortening and area changes if quantitative data on strain and area changes are incorporated for both the competent and incompetent units. Similarly, it may he possible to incorporate variations in detachment depth into the method of Groshong and Epard (1994) and Epard and Groshong (1995) if both original stratigraphic thickness and final detachment depth are known. The two approaches would essentially converge if individual units within a fold were area balanced, which would require knowing original stratigraphic thickness and deformed thickness and detachment depth throughout the fold, including the bounding synclines. This requires that the fold geometry be completely known at the outset, a condition that, for practical reasons, is very rarely attainable.

The more data that are required to achieve a match with natural folds, the less value that geometric models have for the reconstruction of unknown parts of natural folds, such as depth to detachment. Nonetheless, by allowing the effects of individual assumptions to be isolated and tested against natural folds, geometric models retain considerable value for assessing how folds actually grow.

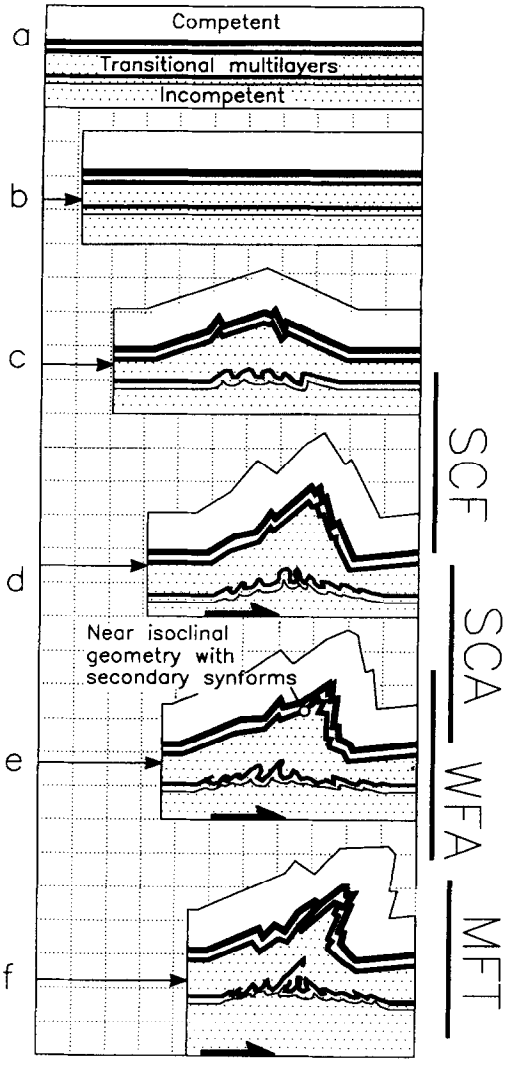

Fig. 14. Schematic diagram of the evolution of a typical detachment fold in the northeastern Brooks Range, showing variation in detachment depth due to changes in the structural thickness of the incompetent unit. Vertical bars represent the approximate developmental stage of the observed folds. (a) Original stratigraphic succession. (b) Period of layer-parallel shortening. (c) Early phase of fixed-hinge folding with negative $A_{\Delta D}$ ($D_o > D_f$), parasitic fixed-hinge folds in transitional units, and disharmonic folds in isolated competent beds. (d) Intermediate phase of folding with $A_{\Delta D} = 0$ ($D_o = D_f$). (e) Later phase of folding with positive $A_{\Delta D}$ ($D_o < D_f$), tightening of folds, especially at the contact between competent and incompetent units in the anticlinal hinge, and area loss due to solution cleavage in fold cores. (f) Highly evolved detachment fold with large positive $A_{\Delta D}$ and thrust faults in core and backlimb.

GENERALIZED DETACHMENT FOLD EVOLUTION

The folds observed in the northeastern Brooks Range define a range in geometry and complexity of anticlines, and their geometry and distribution of strain indicators suggest variable detachment depth and fixed-hinge kinematics. Consequently, we can use these examples, together with the variable detachment depth model, as a guide to describe the evolution of a generalized, fixed-hinge detachment fold. Figure 14 shows the evolution of such a fold, including layer-parallel shortening, parasitic and disharmonic folding, and variations in detachment depth. This figure is not a balanced model, but rather is a schematic illustration of the geometric variation that we think is typical in the evolution of detachment folds in the northeastern Brooks Range.

Initial shortening is taken up in each unit by layer-parallel shortening (stage b). In early, open-geometry folds (stage c), fold area is greater than displaced area (negative area differential) and increases with increasing shortening. This requires transport of incompetent material into the anticlinal core, which results in a decrease in synclinal elevation and detachment depth. In such cases, constant-depth models would overestimate the depth to detachment beneath the fold, as with the Straight Creek fold. Layer-parallel shortening and fold

asymmetry reduce the area increase (Fig. 8), and the effect of area increase on fold geometry decreases with greater relative thickness of the incompetent unit. As the fold evolves, parasitic and disharmonic folds develop, with their size and abundance depending on the percentage of incompetent rock and the average bed thickness (Ramsay and Huber, 1987).

As shortening increases, a point is reached beyond which fold area begins to decrease, resulting in transport of incompetent material out of the anticlinal core and a consequent increase in synclinal elevation and detachment depth (the geometry of the Straight Creek fold suggests that it is at this stage). As fold area decreases, it eventually equals displaced area (area differential is zero, just beyond stage d), so that the final depth equals original thickness. Only at this stage of development can a fixed-hinge, variable-depth fold, for a 'geologic instant', successfully be described using a geometric model that assumes constant depth and migrating hinges.

As the fold tightens further and its area continues to decrease, displaced area exceeds fold area (positive area differential, stage e) and the difference between the two increases with increased shortening. Thus, the final depth beneath the fold exceeds the original depth and constant-depth models would underestimate the depth to detachment beneath the fold, as with the Salisbury Creek anticline. In addition to thickening of the incompetent unit, the fold may lose area during continued tightening by non-plane strain, either through flow of the incompetent unit or of material in solution. Penetrative deformation in the core of the Salisbury Creek anticline likely resulted in area loss by solution. The detachment fold schematically illustrated in Fig. 6 is at approximately stage e of this fold evolution.

With increased shortening, hinge zones of folds in the anticlines are penetratively deformed as interlimb angles decrease to tight-to-isoclinal geometry (stage e to f), as observed along the Marsh Fork transect. Very tight geometries in the Salisbury Creek anticline, West Fork anticline, and Marsh Fork transect are present only in the anticlinal hinge at the competent–incompetent contact and may represent the onset of isoclinal 'lift-off' folding (Mitra and Namson, 1989) (stage f). The area differential of such folds quickly increases as they are elevated above the original elevation of the contact between the competent and incompetent units (stage f). Thrust faults (e.g. stage f) may cut through the fold at any stage of its history, depending on the structural behavior of the subdetachment unit, the locking angle of the dominant member (Ramsay, 1974), and/or fold asymmetry. For example, part of the West Fork anticline was truncated at least by stage c by a thrust cutting up from the subdetachment unit.

CONCLUSIONS

Detachment folds in the northeastern Brooks display a range of geometries and constraints on kinematic evolution. The principal conclusions of this study are:

Table 3. Principal results of analyses of the folds in the northeastern Brooks Range, summarized from Table 2

Detachment fold	Final: initial detachment depth	Uplifted: displaced area	Net area change (ΔA_v)
SCF	$D_f < D_o$	$A_f > A_o$	small gain
WFA*	$D_f = D_o$	$A_f > A_o$	large gain
SCA	$D_f > D_o$	$A_f < A_o$	small loss
MFT	$D_f > D_o$	$A_f < A_o$**	large loss**

*The depth to detachment beneath the WFA is uncertain, but D_f is assumed to equal D_o. **Areas not quantified for MFT.

(1) The distribution and intensity of strain indicators and minor structures indicate that the folds formed by fixed-hinge kinematics in the competent unit (Fig. 6).

(2) Direct observations and analysis using the variable detachment depth model indicate that the structural thickness of the incompetent unit (detachment depth) varied during fold evolution (Tables 2 & 3).

(3) All of the observed folds display a discrepancy ($A_{\Delta D}$) between the actual area observed (or inferred, as with the West Fork anticline) within the anticline (A_f) and the displaced area (A_o, calculated as the product of shortening and the original thickness of the incompetent unit) (Tables 2 & 3). The observed difference between the stratigraphic thickness of the detachment unit (D_o) and the observed final detachment depth (D_f) can account for this discrepancy at least in part. A separate discrepancy (ΔA_v) between the area observed beneath the anticline and that calculated using the variable-depth method (Tables 2 & 3) suggests some combination of layer-parallel shortening of the competent unit, transport of material through synclines (i.e. a local discrepancy between shortening in the competent and incompetent units), non-plane strain by structural transport and/or solution, and/or depositional variability in the original thickness of the incompetent unit at each fold.

(4) Observations indicate that competency contrasts in a stratigraphic sequence (rheology, bed thickness, and relative abundance of strong beds) control fold geometry in detail, including the size and spacing of folds and the role of small-scale structures and penetrative strain. Normal stratigraphic variations and gradations within and between the primary competent and incompetent units may lead to the formation of fixed-hinge parasitic folds, especially near the contact between the competent and incompetent units, and disharmonic folds in the incompetent unit.

(5) Simple geometric models, including the variable detachment depth model, do not take into account all of the many variables required to describe natural fold geometries fully. Thus, such models are more useful for assessing the role of specific variables in fold growth than for the reconstruction of unknown aspects of fold geometry.

(6) This study suggests evolution of typical

detachment folds according to the following scenario (Fig. 14): Folds initially buckle with the hinges fixed with respect to the rock. A rapid increase in anticline area is accommodated by material transport into the core and a decrease in incompetent unit thickness beneath synclines. Anticlines reach a maximum area at an interlimb angle of about 90°. As an anticline tightens, the fold area decreases, at least in part by formation of solution cleavage in fold cores. The fold may respond to continued tightening by thickening of the incompetent unit, transport of material out of the plane of section, and/or lift-off folding. The fold may be truncated by a thrust fault at any time, depending on the local structure.

Acknowledgements—This paper is based in part on a Ph.D. study by Homza, supervised by Wallace. The project was supported by NSF grant EAR-9304482, grants to the Tectonics and Sedimentation Research Group at the University of Alaska from Amoco, ARCO, BP (Alaska), Chevron, Elf, Exxon, Japan National Oil Corp., Mobil, Murphy, Phillips, Shell, Texaco, and Unocal, and to Homza from the Graduate Resource Fellowship, Geist Fund, and Austin Cooley Fund of the University of Alaska Fairbanks. We thank Eric Erslev, Rick Groshong, Cathy Hanks, Chris Hedlund, Paul Layer, and Lew Shapiro for their helpful reviews of the manuscript.

REFERENCES

Anderson, A. V., Wallace, W. K. and Mull, C. G. (1994) Depositional record of a major tectonic transition in northern Alaska: Middle Devonian to Mississippian rift-basin margin deposits, upper Kongakut River region, eastern Brooks Range, Alaska. In *Proceedings of the International Conference on Arctic Margins*, eds D. Thurston and K. Fujita, pp. 71–76. US Department of the Interior, Minerals Management Service Outer Continental Shelf Study, 94-0040.

Banks, C. J. and Warburton, J. (1986) 'Passive-roof' duplex geometry in the frontal structures of the Kirthar and Sulaiman mountain belts, Pakistan. *Journal of Structural Geology* **8**, 229–237.

Chamberlin, R. T. (1910) The Appalachian folds of central Pennsylvania. *Journal of Geology* **18**, 228–251.

Currie, J. B., Patnode, H. W. and Trump, R. P. (1962) Development of folds in sedimentary strata. *Geological Society of America Bulletin* **73**, 655–674.

Dahlstrom, C. D. A. (1990) Geometric constraints derived from the law of conservation of volume and applied to evolutionary models for detachment folding. *American Association of Petroleum Geologists Bulletin* **74**, 336–344.

Epard, J.-L. and Groshong, R. H. (1995) Kinematic model of detachment folding including limb rotation, fixed hinges and layer-parallel strain. *Tectonophysics* **247**, 85–103.

Fischer, M. P., Woodward, N. B. and Mitchell, M. M. (1992) The kinematics of break-thrust folds. *Journal of Structural Geology* **14**, 451–460.

Groshong, R. H. and Epard, J.-L. (1994) The role of strain in area-constant detachment folding. *Journal of Structural Geology* **16**, 613–618.

Hardy, S. and Poblet, J. (1994) Geometric and numerical model of progressive limb rotation in detachment folds. *Geology* **22**, 371–374.

Homza, T. X. (1992) A detachment fold-truncation duplex southwest of Bathtub Ridge-northeastern Brooks Range, Alaska. Unpublished M.S. thesis, University of Alaska, Fairbanks.

Homza, T. X. (1993) Preliminary observations of the Straight Creek detachment anticline-northeastern Brooks Range, Alaska: a basis for geometric and kinematic detachment fold models. *Alaska Division of Geological and Geophysical Surveys Public Data File* 93-43.

Homza, T. X. (1994) The structural geometry of detachment folds above a duplex in the Franklin Mountains, northeastern Brooks Range, Alaska. *Alaska Division of Geological and Geophysical Surveys Public Data File* 94-43.

Homza, T. X. (1995) Detachment folds of the northeastern Brooks Range, Alaska-A basis for geometric and kinematic models of detachment folds. Unpublished Ph.D. thesis, University of Alaska, Fairbanks.

Homza, T. X. and Wallace, W. K. (1995) Geometric and kinematic models for detachment folds with fixed and variable detachment depths. *Journal of Structural Geology* **17**, 475–588.

Imm, T. A., Dillon, J. T. and Bakke, A. A. (1993) Generalized geologic map of the Arctic National Wildlife Refuge, northeastern Brooks Range, Alaska. *Alaska Division of Geological and Geophysical Surveys, Special Report* 42.

Jamison, W. R. (1987) Geometric analysis of fold development in overthrust terranes. *Journal of Structural Geology* **9**, 207–219.

LePain, D. L. (1993) Transgressive sedimentation in rift-flank region: deposition of the Endicott Group (Early Carboniferous), northeastern Brooks Range, Alaska. Unpublished Ph.D. Thesis, University of Alaska, Fairbanks.

LePain, D. L., Crowder, R. K. and Wallace, W. K. (1994) Early Carboniferous transgression on a passive continental margin: Deposition of the Kekiktuk Conglomerate, northeastern Brooks Range, Alaska. *American Association of Petroleum Geologists Bulletin* **78**, 679–699.

Marshak, S. and Mitra, G. (1988) *Basic Methods of Structural Geology*. Prentice Hall, Englewood Cliffs, N.J.

Mitra, S. (1990) Fault-propagation folds: geometry, kinematic evolution, and hydrocarbon traps. *Bulletin of the American Association of Petroleum Geologists* **74**, 921–945.

Mitra, S. and Namson, J. S. (1989) Equal-area balancing. *American Journal of Science* **289**, 563–599.

Moore, T. E., Wallace, W. K., Bird, K. J., Karl, S. M., Mull, C. G. and Dillon, J. T. (1994) Chapter 3: Geology of northern Alaska. In *The Geology of Alaska*, eds G. Plafker and H. C. Berg, pp. 49–140. The Geology of North America, Geological Society of America, Boulder, Colorado G1.

Namson, J. S. and Wallace, W. K. (1986) A structural transect across the northeastern Brooks Range, Alaska. *Geological Society of America, Abstracts with Programs* **18**, 163.

Poblet, J. and Hardy, S. (1995) Reverse modelling of detachment folds; application to the Pico del Aguila anticline in the South Central Pyrenees (Spain). *Journal of Structural Geology* **17**, 1707–1724.

Poblet, J. and McClay, K. (1996) Geometry and kinematics of single-layer detachment folds. *American Association of Petroleum Geologists Bulletin* **80**, 1085–1109.

Ramsay, J. G. (1974) Development of chevron folds. *Bulletin of the geological Society, America* **85**, 1741–1754.

Ramsay, J. G. and Huber, M. I. (1983) *The Techniques of Modern Structural Geology, Volume 1: Strain Analysis*. Academic Press, New York.

Ramsay, J. G. and Huber, M. I. (1987) *The Techniques of Modern Structural Geology, Volume 2: Folds and Fractures*. Academic Press, New York.

Rowan, M. G. and Kligfield, R. (1992) Kinematics of large-scale asymmetric buckle folds in overthrust shear: an example from the Helvetic nappes. In *Thrust Tectonics*, ed. K. R. McClay, pp. 165–174. Chapman and Hall, London.

Suppe, J. (1983) Geometry and kinematics of fault-bend folding. *American Journal of Science* **283**, 684–721.

Suppe, J. and Medwedeff, D. A. (1990) Geometry and kinematics of fault-propagation folding. *Eclogae Geologicae Helvetiae* **83**, 409–454.

Wallace, W. K. (1993) Detachment folds and a passive-roof duplex: Examples from the northeastern Brooks Range, Alaska. In *Short Notes on Alaskan Geology (1993)*, ed. Solie and Tannian, pp. 81-99. Alaska Div. Geol. and Geophys. Surv. Professional Report 113.

Wallace, W. K. and Hanks, C. L. (1990) Structural provinces of the northeastern Brooks Range, Arctic National Wildlife Refuge, Alaska. *American Association of Petroleum Geologists Bulletin* **74**, 1100–1118.

Wiltschko, D. V. and Chapple, W. M. (1977) Flow of weak rocks in the Appalachian Plateau folds. *American Association of Petroleum Geologists Bulletin* **61**, 653–670.